Editors' Suggestion

# Electric-Field-Induced Pattern Formation in Layers of DNA Molecules at the Interface between Two Immiscible Liquids

Steffen Hardt,[1,*] Johannes Hartmann,[1] Sicheng Zhao,[1] and Aditya Bandopadhyay[2]
[1]Institute for Nano- and Microfluidics, TU Darmstadt, Alarich-Weiss-Straße 10, D-64287 Darmstadt, Germany
[2]Department of Mechanical Engineering, Indian Institute of Technology Kharagpur, Kharagpur, West Bengal, India—721302

(Received 16 May 2019; revised manuscript received 25 October 2019; accepted 17 December 2019; published 12 February 2020)

The concentration patterns of DNA molecules attached to the interface between two immiscible aqueous phases forming under an electric field are studied. The pattern formation is driven by hydrodynamic interactions between the molecules originating from the electro-osmotic flow due to the Debye layer around a molecule. A nonlinear integrodifferential equation is derived describing the time evolution of the concentration field at the liquid-liquid interface. A linear stability analysis of this equation shows that a mode of given wavelength is initially stable, but destabilizes after a critical time which is inversely proportional to the wavelength. The scaling behavior of the critical time with electric field strength and viscosity found in the experiments agrees with the predictions by the theoretical model.

DOI: 10.1103/PhysRevLett.124.064501

In the past decades, electric-field-induced pattern formation in suspensions has been the focus of intense research activities. Probably the most well-known example in that context is the chain and column formation in suspensions of microparticles and colloidal suspensions, especially in electrorheological fluids [1–3]. The driving mechanism behind the pattern formation is the dipole-dipole interaction between the particles. However, in experiments it is often not easily possible to study systems with pure dipolar interactions, since other effects such as hydrodynamic interactions may come into play [2]. In fact, hydrodynamic interactions were identified as the driving mechanism behind a number of other patterns spontaneously forming in suspensions when an electric field is applied. An example is the pattern formation in colloidal dispersions due to electrohydrodynamic (EHD) flow, which is caused by a modulation of the (complex) dielectric permittivity in those regions occupied by particles [4,5]. Similar phenomena occur when metallic microparticles are dispersed in a weakly conducting liquid [6,7]. Pattern formation is also observed when particles are electrophoretically deposited on an electrode. Different mechanisms were proposed to explain the emerging structures, either electrokinetic flows originating from the electric double layer (EDL) around the particles [8,9] or electrokinetic flows originating from the distortion of the EDL at the electrode [10]. Recently, it was reported that ion exchange resin particles sedimented to a charged surface interact and assemble via self-generated electric fields [11]. Some of these phenomena bear resemblance to the collective motion of microswimmers that may also manifest itself in pattern formation (for an overview, see Ref. [12]). Pattern formation also occurs at fluid interfaces. When an electric field is applied to microparticles attached to a liquid surface or to a liquid-liquid interface, they experience an interaction force that can give rise to regular patterns [13–15]. In this case, the capillary interaction between the particles due to the electrodipping force plays a key role [16–18].

In this Letter, we report that similar phenomena as those described above also occur when the particles are replaced by polyelectrolytes, specifically DNA molecules. Characteristic patterns in the DNA concentration field develop when the molecules are attached to the liquid-liquid interface in an aqueous two-phase system (ATPS) as well as at the three-phase contact line of an ATPS wetting a solid surface. The evolution of the concentration field is described using a continuum-mechanical theory.

A schematic of the experimental setup is shown in Fig. 1; details can be found in the Supplemental Material (see Sec. 1.1 [19]). In brief, the ATPS is contained in a glass tube. The buffer solution reservoir is filled with sodium phosphate buffer solution. The same buffer solution is used to dissolve polyethylene glycol (PEG) and dextran that form a two-phase system with the composition 12.5% $w/w$ dextran, 10% $w/w$ PEG, and 77.5% $w/w$ buffer solution for the reference case. To prepare the ATPS, all components were mixed and are allowed to separate. The dextran phase and the PEG phase were then pipetted into different tubes, and YOYO-1 stained $\lambda$-DNA was added to the dextran phase. Subsequently, the two liquids were filled into the glass tube, with the denser dextran phase forming the bottom layer. A dc electric field was applied between two electrodes, one dipped into the PEG phase, the second into the buffer reservoir. Salt bridges between the buffer reservoir and the dextran phase ensure that no bubbles are introduced into the liquid, while electric current may pass. The concentration of DNA molecules was imaged

 

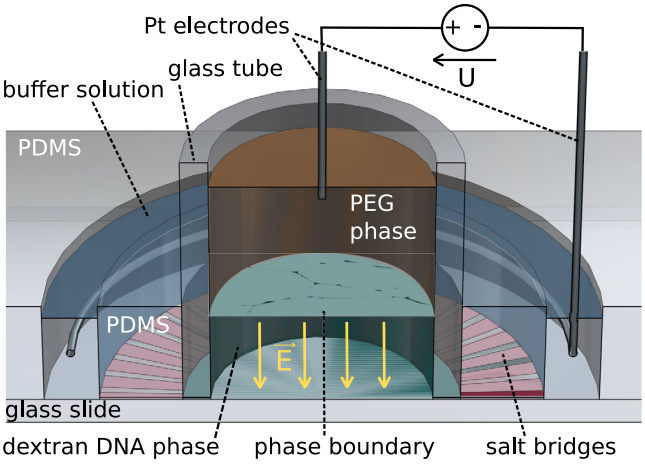


FIG. 1. Schematic of the experimental setup used to study DNA concentration patterns at the liquid-liquid interface in an ATPS. The patterns are imaged through the glass slide at the bottom.

through the glass slide based on epifluorescence microscopy with a 2× objective that was focused on the liquid-liquid interface. To obtain one data point of the results reported below, the corresponding experiment was performed at least 5 times. As soon as the electric field is switched on, electrophoretic motion of the DNA molecules toward the liquid-liquid interface sets in. The molecules attach to the interface, presumably because they get trapped in an electrostatic potential well, as described by Hahn *et al.* [23]. After a certain time concentration patterns become visible at the interface consisting of filaments [Fig. 2(a)]. The filaments display a number of clusters that grow as time progresses, whereas the filaments become thinner. After a while the clusters have become the most prominent features of the pattern [Fig. 2(b)]. The clusters merge as time progresses, leading to an increase of the average distance between clusters. Increasing the applied voltage results in a decrease of the characteristic scale of the patterns at a given point in time [Figs. 2(b)–2(d)]. A more detailed and more quantitative analysis of the evolution of the concentration patterns is available from the Supplemental Material [19], as well as a video showing a characteristic pattern evolution. To investigate the physics behind the pattern formation, we performed additional experiments in a microfluidic chip, schematically shown in Fig. 3(a). With this setup it is possible to inspect the liquid-liquid interface from a direction perpendicular to the electric field. In experiments with the same liquids as in the previous experiments, DNA concentration patterns and clusters at the interface are observed as well. Recirculating flows emerge in the vicinity of the clusters, visible in Fig. 3(b) as trace lines of DNA molecules advected with the flow. Confocal microscopy images show that these clusters are found close to the three-phase contact lines at the top and bottom walls of the microfluidic channels. These results clearly indicate that DNA molecules attached to the

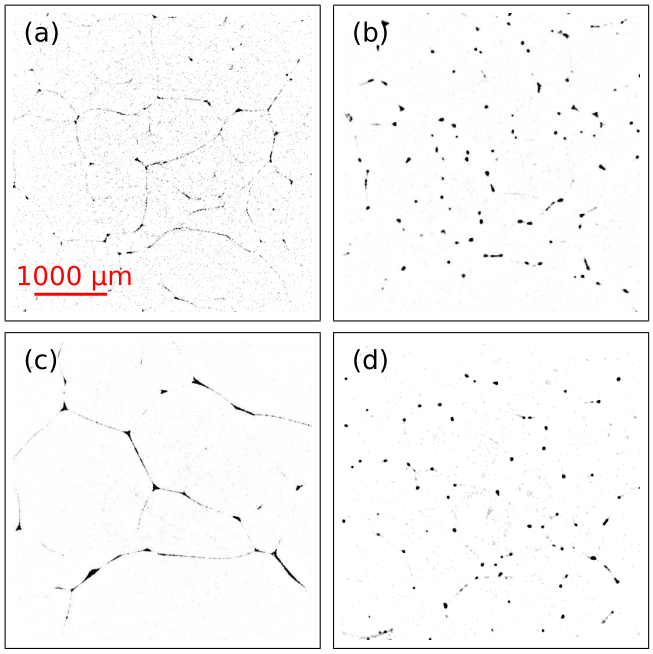


FIG. 2. Fluorescence microscopy images of patterns in the DNA concentration field at the liquid-liquid interface. (a) ($t = t_0$, $U = 30$ V) and (b) ($t = 2.2t_0$, $U = 30$ V) show the variation of the patterns with time. $t$ is the time that has passed after applying the voltage, and $t_0$ indicates the experimentally determined time of pattern formation (see Sec. 1.4 in Ref. [19]). (b),(c) ($t = 2.2t_0$, $U = 10$ V) and (d) ($t = 2.2t_0$, $U = 20$ V) demonstrate the variation of the patterns with applied voltage. The gray scale map of the original fluorescence micrographs was inverted for better visibility.

liquid-liquid interface give rise to a flow. Figure 3(c) shows a schematic of the flow field around a molecule at the interface. The flow along the interface is towards the molecule and gets redirected into a jetlike structure normal to the interface. Such a flow field induces an attractive hydrodynamic interaction between two molecules attached to the interface. The flow away from the boundary resembles the structures emerging in other hydrodynamic instabilities in slab geometries. The most prominent of these is probably the Rayleigh-Bénard (RB) instability which is driven by buoyancy forces when the fluid in the slab is heated from below [24]. When a threshold in the temperature difference is reached, the homogeneous state breaks down, and convection cells are formed. This means that a small perturbation around the homogeneous state triggers an instability, e.g., a perturbation of the temperature field. This is analogous to the situation studied in our work where a small perturbation of the concentration field triggers an instability. The RB system is known for its ordered arrays of convection cells. Cellular structures can also be found in the DNA concentration patterns (cf. Fig. 2), but they appear less regular than the typical RB patterns. To formulate a theoretical model capturing the physics of pattern formation we assume that the liquid-liquid interface coincides with the

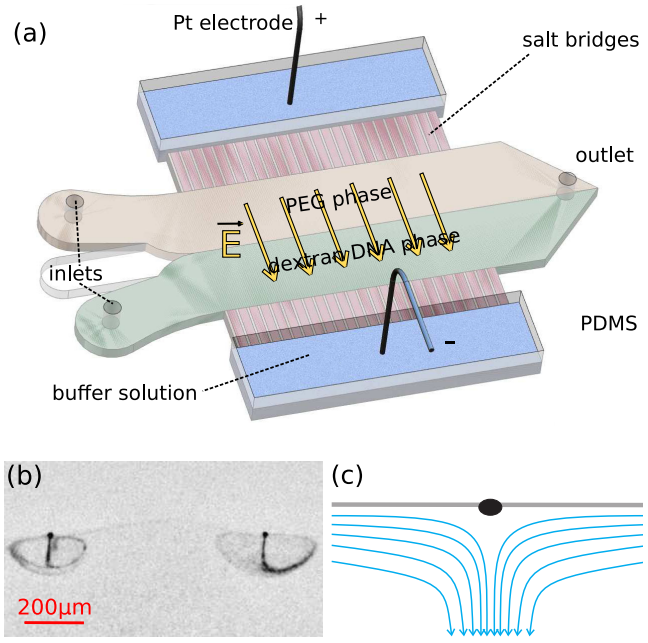


FIG. 3. (a) Schematic of an alternative experimental setup used to visualize the recirculating flow field around DNA clusters. The viewing direction is perpendicular to the electric field. (b) Traces of DNA molecules in a recirculating flow field around two clusters close to the liquid-liquid-solid contact line. The gray scale map of the original fluorescence micrographs was inverted for better visibility. (c) Schematic representation of the flow field around a DNA molecule attached to the interface.

$(x, y)$ plane. The molar concentration field of molecules attached to the interface is given by $n(x, y)$. We assume pointlike molecules that can only move within the $(x, y)$ plane. The molecules are charged, therefore an EDL forms around them, counterbalancing the molecular charge. In the framework of our model we also neglect the spatial extension of the EDL. Via the net charge of the EDL the electric field, pointing in the $z$ direction, exerts a force on the liquid, giving rise to a flow field $\mathbf{u}$. The flow field in each of the two phases is governed by the Stokes equation

$$\eta\nabla^2\mathbf{u} - \nabla p + \mathbf{f} = 0, \tag{1}$$

where $\eta$ is the dynamic viscosity of the liquid, $p$ the pressure field, and $\mathbf{f}$ is the force density due to the EDL. This has to be solved together with the incompressibility constraint $\nabla \cdot \mathbf{u} = 0$. The force density due to an ensemble of molecules is proportional to the molecular number density $n(x, y)$. We first consider the flow field due to a single molecule, located inside the dextran phase at a position $(x, y, z) = (x_0, y_0, \varepsilon)$. In the experiments described above, the viscosity ratio between the two liquids is $\eta_{\mathrm{dex}}/\eta_{\mathrm{PEG}} \approx 2$, but as a simplifying case, we assume a very large viscosity ratio. Based on that, the boundary conditions for the flow at the liquid-liquid interface are given as

$$u_z|_{z=0} = 0, \qquad \left.\frac{\partial u_x}{\partial z}\right|_{z=0} = 0, \qquad \left.\frac{\partial u_y}{\partial z}\right|_{z=0} = 0. \tag{2}$$

We are interested in the flow field for $z \geq 0$. For simplicity, the influence of the wall at the bottom is neglected. To guarantee that the no-shear stress boundary condition at the liquid-liquid interface is fulfilled, we employ the method of images. That is, for every molecule sitting at $z = \varepsilon$ there is one at $z = -\varepsilon$, producing a flow field which is the mirror image of the one inside the domain. For a single molecule at position $\mathbf{r}_0$, the source distribution is given by $\mathbf{f} = \mathbf{g}\delta(\mathbf{r} - \mathbf{r}_0)$, with $\mathbf{g} = (0, 0, g)$. We have $g \propto qE$, where $q$ is the charge of a molecule and $E$ the electric field strength. The flow field due to this pointlike source in an unbounded medium is the well-known Stokeslet

$$\mathbf{u}(\mathbf{r}) = \frac{1}{8\pi\eta}\mathbf{g} \cdot \left[\frac{\mathbf{I}}{|\mathbf{R}|} + \frac{\mathbf{R} \otimes \mathbf{R}}{|\mathbf{R}|^3}\right], \tag{3}$$

where, referring to the experiment $\eta \equiv \eta_{\mathrm{dex}}$, $\mathbf{I}$ is the unit tensor, and $\mathbf{R} = \mathbf{r} - \mathbf{r}_0$. The evolution equation for the concentration field $n(x, y)$ only requires the projection of the velocity field to the liquid-liquid interface at $z = 0$, $\mathbf{u}_{\mathrm{p}}$. For a single molecule at $z = \varepsilon$, this projection is given by

$$\mathbf{u}_p^{(\varepsilon,g)}(\mathbf{r}) = -\frac{g\varepsilon}{8\pi\eta}\frac{\mathbf{R}}{|\mathbf{R}|^3}. \tag{4}$$

To fulfill the boundary conditions at $z = 0$, an image flow field due to a source at $z = -\varepsilon$ has to be added:

$$\mathbf{u}_p(\mathbf{r}) = \mathbf{u}_p^{(\varepsilon,g)}(\mathbf{r}) + \mathbf{u}_p^{(-\varepsilon,-g)}(\mathbf{r}) = -\frac{g\varepsilon}{4\pi\eta}\frac{\mathbf{R}}{|\mathbf{R}|^3}. \tag{5}$$

To model a molecule attached to the liquid-liquid interface we take the limit $\varepsilon \to 0$. To obtain a finite flow field, we need a source scaling as $g = \gamma/\varepsilon$, from which we obtain

$$\lim_{\varepsilon\to 0}\mathbf{u}_p(\mathbf{r}) = -\frac{\gamma}{4\pi\eta}\frac{\mathbf{R}}{|\mathbf{R}|^3}, \tag{6}$$

with $\mathbf{R} = (x - x_0, y - y_0, 0)$. The total flow field at the liquid-liquid interface $\mathbf{U}_p(\mathbf{r})$ originates from many such doublets of points sources distributed along the interface with a number density of $n$. Assuming an infinitely extended liquid-liquid interface, we obtain

$$\mathbf{U}_p(x, y) = -\frac{\gamma}{4\pi\eta}\int_{-\infty}^{\infty}\int_{-\infty}^{\infty}\frac{n(x_0, y_0)}{[(x - x_0)^2 + (y - y_0)^2]^{3/2}} \times \begin{pmatrix} x - x_0 \\ y - y_0 \end{pmatrix} dx_0 dy_0. \tag{7}$$

The integrand has a singularity at $(x_0, y_0) = (x, y)$, so the above expression is to be interpreted as a Cauchy principal value. Based on the physically reasonable assumption of a

finite concentration field $n$ that vanishes at infinity, it can be shown that the principal value integral is a finite expression. The evolution of the concentration field at the interface is determined by an advection-diffusion equation of the form

$$\frac{\partial n(\mathbf{r},t)}{\partial t}+\nabla_s\cdot[n(\mathbf{r},t)\mathbf{U}_p(\mathbf{r},t)]-D\nabla_s^2 n(\mathbf{r},t)=S(\mathbf{r},t), \quad (8)$$

where $\mathbf{r}$ is a point at the interface and $\nabla_s \equiv [(\partial/\partial x),(\partial/\partial y)]$. Apart from the advective transport of molecules, diffusive transport with an interfacial diffusion coefficient of $D$ is taken into account. The source term $S(\mathbf{r},t)$ represents molecules that attach to or detach from the interface. In the experiments described above, adsorbed molecules stay at the interface, but the patterns already start developing while still molecules from the dextran phase electromigrate to the interface. Molecular interactions (which are usually short-range interactions such as van der Waals, screened electrostatic, or entropic interactions) are not accounted for in Eq. (8). This means that we expect the equation to be valid for concentrations so small that the average distance between two molecules is lower than the range of the interactions. Equation (8) constitutes a nonlinear integrodifferential equation for the concentration field that can usually only be solved numerically. It is not difficult to show that for a spatially constant concentration field $n$, the flow field $\mathbf{U}_p$ vanishes. Only when an inhomogeneity in the concentration field is present, a flow field emerges. A region of increased concentration gives rise to a flow field of the same structure as shown in Fig. 3(c). Such a region pulls further molecules in along the interface, leading to a further increase in concentration and demonstrating the self-amplifying character of small perturbations in the concentration field.

One can perform a linear stability analysis to determine how a perturbation of the concentration field evolves in time. For the specific scenario considered in the experiments, the source term is constant and given by $S = n_b\mu_e E$, where $E$ is the electric field strength, $n_b$ the molar concentration of DNA molecules in the dextran phase, and $\mu_e$ is the electrophoretic mobility of the molecules. To perform a linear stability analysis, the molar concentration at the interface is written as $n(\mathbf{r},t) = N(t) + n'(\mathbf{r},t)$, where $n'$ is a small perturbation written in the form

$$n'(\mathbf{r},t) = a(t)\exp(\mathrm{i}kx). \quad (9)$$

The concentration in the base state is given by $N(t) = n_b\mu_e E t$, reflecting the electrophoretic transport of molecules to the interface by an $E$ field switched on at $t = 0$. Since the base state is homogeneous, we can, without loss of generality, assume a plane-wave perturbation in the $x$ direction, as in Eq. (9). The linear stability analysis (see Sec. 3 in the Supplemental Material [19]) results in

$$a(t) = a_0\exp\left(-k^2Dt + k\frac{\gamma n_b\mu_e E}{4\eta}t^2\right), \quad (10)$$

with the mode-dependent growth rate given by $-k^2D + k(\gamma n_b\mu_e E/2\eta)t$. From the first term of this expression we infer that diffusion dampens the instability, as expected. We also find that initially all modes are stable, i.e., the growth rate is negative. At a critical time

$$t_c = \frac{4\eta D}{\gamma n_b\mu_e E}k \quad (11)$$

the modes start to destabilize [19]. We have the complex situation that long-wavelength (short-wavelength) modes destabilize fast (slowly), but after destabilization their growth rate is slow (fast). Therefore, a simple picture identifying the most unstable modes that dominate the instability is lacking.

For comparison between the theoretical and the experimental results it suggests itself to consider the critical time. According to Eq. (11), this scales as $t_c \propto E^{-2}$, since $\gamma \propto E$. Moreover, by taking into account the Einstein-Smoluchowski relation for the electrophoretic mobility, we obtain $t_c \propto \eta$. In the experiments, performed with the setup shown in Fig. 1, pattern formation already sets in when DNA molecules are still electromigrating toward the interface. Therefore, the first inhomogeneities in the concentration field at the liquid-liquid interface are impossible to capture, since the fluorescence in the bulk dextran solution dominates the one originating from the interface. Instead, the concentration patterns only become visible when they are already well developed, i.e., at a time $t_0 = t_c + \Delta t$, the experimentally observed pattern formation time.

Figure 4 shows the results of a parameter study in which the applied voltage $U$ and the viscosity $\eta$ were varied. The viscosity was varied by studying ATPSs with different polymer concentrations. $t_0$ was determined using an in-house MATLAB code (see Sec. 1.4 in Ref. [19]). In the main diagram, the variation of $t_0$ with $U$ is displayed, while the inset shows the variation with $\eta$. The experimental data appear as symbols, while the theoretical predictions appear as lines. Considering the relationship between $t_0$ and $t_c$ and the scaling relationships predicted by the stability analysis, the model functions $A_1/U^2 + B_1$ and $A_2\eta + B_2$ were employed, subjected to the constraint $B_1 = B_2$. Gaussian least squares fits were used to determine the model parameters. Figure 4 shows that the experimental data agree well with the scaling relationships derived from the theoretical model.

Via Eq. (11), the fit parameters $A_1$ and $A_2$ are related to the model parameters. Both fit parameters contain $\gamma$, which is very difficult to determine since this quantity encodes information about the position of a DNA molecule relative to the liquid-liquid interface. To eliminate $\gamma$, we consider the ratio $A_1/A_2$, which, according to theory, should be

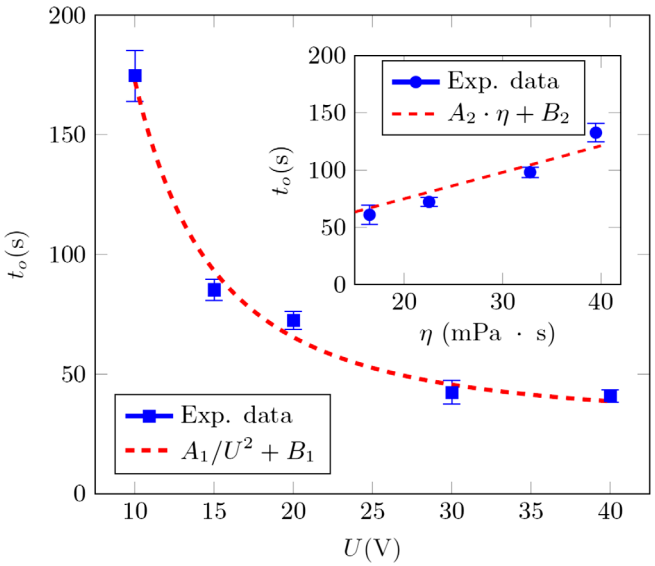


FIG. 4. Main diagram: Time of pattern formation $t_0$ as a function of the applied voltage $U$ for a fixed dextran phase viscosity of 22.5 mPa s. Inset: The same, but as a function of $\eta$, for a fixed applied voltage of 20 V. The symbols represent the experimental data, the curves the scaling relations obtained from the theoretical model. The error bars represent the standard error of the mean.

equal to $\eta U^2$. Based on the fitted values, we obtain 6504 $V^2$ mPas for this ratio, compared to 9000 $V^2$ mPas for the theoretical value. Given the simplifications underlying the theoretical expression such as linearization or the assumption of an inviscid PEG phase, we consider this a good agreement between experiments and theory.

To conclude, we have shown that concentration patterns of DNA molecules attached to a liquid-liquid interface are formed under an electric field. The pattern formation is driven by hydrodynamic interactions between the molecules originating from the electro-osmotic flow due to the Debye layer around a molecule. The spatiotemporal evolution of the concentration field is described by a nonlinear partial integrodifferential equation. A linear stability analysis of this equation shows that long-wavelength (short-wavelength) modes destabilize fast (slowly), but after destabilization their growth rate is slow (fast). The predicted scaling of the critical time at which the instability sets in with electric field strength and viscosity is confirmed by experimental data.

The authors wish to acknowledge the support of this work by the German Research Foundation, Grants No. HA2696/37-1 and No. HA2696/43-2, as well as helpful discussions with Aaron D. Ratschow. A. B. acknowledges financial support by the Alexander von Humboldt Foundation.

S. H. and J. H. contributed equally to this work.

*hardt@nmf.tu-darmstadt.de

[1] J. E. Martin, J. Odinek, and T. C. Halsey, Phys. Rev. Lett. **69**, 1524 (1992).
[2] A. Kumar, B. Khusid, Z. Qiu, and A. Acrivos, Phys. Rev. Lett. **95**, 258301 (2005).
[3] J. S. Park and D. Saintillan, Phys. Rev. E **83**, 041409 (2011).
[4] M. Trau, S. Sankaran, D. A. Saville, and I. A. Aksay, Langmuir **11**, 4665 (1995).
[5] M. Trau, S. Sankaran, D. A. Saville, and I. A. Aksay, Nature (London) **374**, 437 (1995).
[6] M. V. Sapozhnikov, Y. V. Tolmachev, I. S. Aranson, and W. K. Kwok, Phys. Rev. Lett. **90**, 114301 (2003).
[7] M. V. Sapozhnikov, I. S. Aranson, W. K. Kwok, and Y. V. Tolmachev, Phys. Rev. Lett. **93**, 084502 (2004).
[8] M. Böhmer, Langmuir **12**, 5747 (1996).
[9] Y. Solomentsev, M. Böhmer, and J. L. Anderson, Langmuir **13**, 6058 (1997).
[10] S.-R. Yeh, M. Seulst, and B. I. Shraimang, Nature (London) **386**, 57 (1997).
[11] R. Niu, T. Palberg, and T. Speck, Phys. Rev. Lett. **119**, 028001 (2017).
[12] J. Elgeti, R. G. Winkler, and G. Gompper, Rep. Prog. Phys. **78**, 056601 (2015).
[13] N. Aubry and P. Singh, Phys. Rev. E **77**, 056302 (2008).
[14] N. Aubry, P. Singh, M. Janjua, and S. Nudurupati, Proc. Natl. Acad. Sci. U.S.A. **105**, 3711 (2008).
[15] K. Masschaele and J. Vermant, Soft Matter **7**, 10597 (2011).
[16] L. Foret and A. Würger, Phys. Rev. Lett. **92**, 058302 (2004).
[17] K. D. Danov, P. A. Kralchevsky, and M. P. Boneva, Langmuir **20**, 6139 (2004).
[18] K. D. Danov and P. A. Kralchevsky, J. Colloid Interface Sci. **298**, 213 (2006).
[19] See Supplemental Material at http://link.aps.org/supplemental/10.1103/PhysRevLett.124.064501 for videos showing a characteristic time evolution of the DNA concentration pattern, details of the experimental setup, experimental procedure, image capturing, data acquisition, and details of the linear stability analysis, which includes Refs. [20–22].
[20] T. Hahn, G. Münchow, and S. Hardt, J. Phys. Condens. Matter **23**, 279502 (2011).
[21] A. D. Diamond and J. T. Hsu, Biotechnology Techniques **3**, 119 (1989).
[22] D. Gidaspow and L. Huilin, AIChE J. **44**, 279 (1998).
[23] T. Hahn and S. Hardt, Soft Matter **7**, 6320 (2011).
[24] M. C. Cross and P. C. Hohenberg, Rev. Mod. Phys. **65**, 851 (1993).